



## Corrosion Inhibitors, Molecular Docking and Quantum Chemical Parameters Of Allyl Rhodanine Azodye Derivatives and Developed To Protect C-Steel in Acidic Environments

A.A. El-Sonbaty<sup>a,\*</sup>, A.A. Al-Sarawy<sup>a</sup>, M. Mossad<sup>b</sup>, M.H. Mahmoud<sup>a</sup>

<sup>a</sup>Mathematical and Physical Engineering Department, Faculty of Engineering, Mansoura University, El-Mansoura, Egypt

<sup>b</sup>Public Works Engineering Department, Faculty of Engineering, Mansoura University, Mansoura 35516, Egypt



CrossMark

### Abstract

The inhibitive impact of new environmentally friendly synthesized allyl rhodanine azodye derivatives (1-3) versus C-steel and its performance were detected in 2 molar hydrochloric acid solution utilized mass reduction, Tafel polarization, electrochemical impedance spectroscopy (EIS) and electrochemical frequency modulation (EFM) techniques. The inhibition efficiency percentage (% IE) of these investigated composite is: inhibitor (1) > (2) > (3). The mixed-kind inhibitor allyl rhodanine azodye compounds have isotherm Temkin-following adsorption habits on C-steel. The temperature effect on corrosion protection has been research and the activation thermodynamic was measured. It appears that a decrease in corrosion protection effectiveness with rising temperatures caused the inhibitor to desorb. Utilizing scanning electron microscope and energy dispersive X-ray spectroscopy (SEM-EDX) and the morphology of inhibited C-steel was examined. The data show that the effectiveness of the protection increases with increasing inhibitor doses. The receptor of the breast cancer 3hb5-oxidoreductase was predicted to bind with allyl rhodanine azodye derivatives *via* molecular docking. The data showing a decline in  $E_{HOMO}$  and  $E_{LUMO}$  orders corresponds with an increase in % IE that strengthens the preceding order.

**Keywords:** Corrosion inhibitors, C-steel, Allyl rhodanine azodye, Quantum chemical parameters, Molecular docking, SEM-EDX analysis.

### Introduction

Acid solutions are commonly utilized in manufacturing, including for the pickling of steel and iron in acid, the processing of chemicals for cleaning, the mining sector, and the acidification of well oil [1-4]. As a result, both from the standpoint of production and theoretical data viewer, the development of novel inhibitors modified and the studies with established inhibitors or benchmarking against industry standards would strengthen the assessment of the synthesized compounds' performance and provide context for their potential practical applications as recently reported [5,6].

The best method for preventing acid corrosion has been regarded to be the use of chemical inhibitors [7-9] as a result of the difficulties caused by acid corrosion growing and the need to develop various corrosion control strategies. Some organic substances are primarily used as inhibitors in many sectors, including quaternary ammonium salts, acetylenic alcohol, and heterocyclic compound. The organic composite contains hetero atoms that adsorb on metal surfaces, such as S, O, and N, and a physical barrier is provided with the composite to slow the flow of corrosive substances onto the surface of metal. [10-16]. Other study gives the adsorption process depend on the chemical structure of inhibitors, the type of metal and its charge. These organic compounds include heterocyclic elements with N atoms, which are thought to be effective corrosion inhibitors in acidic environments because they increase corrosion protection, have excellent thermal stability, and reduce obnoxious odor for a variety of metals and alloys in unlike aggressive solutions [13-22]. As a result, both from the standpoint of production and theoretical data viewer, the development of novel inhibitors modified to contain a 4-aminoantipyrineheterocyclic ring The investigation of the relationship between chemical structure and their protective abilities is particularly important.

The research target discovers the inhibition influence and electrochemical habit of newly synthesized allyl rhodanine azodye derivatives (1-3) for C-steel in two molar hydrochloric acid by the mass reduction, electrochemical frequency modulation (EFM), electrochemical impedance spectroscopy (EIS) and Tafel polarization methods. The molecular properties of many types of composites have been protected by a number of quantum-chemistry investigations [23,24]. Given that these allyl rhodanine azodye derivatives do not cause C-steel corrosion in 2 M HCl by formation of a protective coating via adsorption on its exterior, EDX and SEM examinations of the C-steel in 2 M acid surface are performed.

### Experimental

#### Measurements

By using HF tests using a 3-21G basis set, the researched allyl rhodanine azodye derivatives crystal structures are improved. The molecules are paint with Perkin Elmer ChemBiodraw and give by utilized software Perkin Elmer

\*Corresponding author e-mail: [aelsonbaty@hotmail.com](mailto:aelsonbaty@hotmail.com); (Ahmed A. El-Sonbaty).

Receive Date: 20 April 2024, Revise Date: 10 May 2024, Accept Date: 03 June 2024

DOI: [10.21608/EJCHEM.2024.284076.9618](https://doi.org/10.21608/EJCHEM.2024.284076.9618)

©2025 National Information and Documentation Center (NIDOC)

ChemBio3D. Quantum calculations are carried out using the Accelrys (Material Studio Version 4.4) software [23-25]. This investigation parallels the actual docking procedure [26], which evaluates the pair-wise energies of the interactions between the ligand and the protein. The MMFF94 Force used Docking Server to reduce the energy of the ligand molecule. The ligand atoms were receiving partial Gasteiger charges. Rotatable bonds and combined non-polar H atoms were shown. The allyl rhodanine azodye derivatives (1-3) model protein was used for docking experiments. The AutoDock option was used to add the required hydrogen atoms; Kollman unified atom kind charges, and parameters [27]. The application Auto-grid was used to create affinity (grid) maps using 0.375-area,  $20 \times 20 \times 20$ -grid data [28]. In order to continuously measure the electrostatic terms and van der Waals, Autoz-Dock distance-vassal dielectric functions and parameter group were used.

#### Material and Medium

To evaluate corrosion experiments, C-steel was used. Its weight percentage breakdown is 0.20 C, 0.30 Si, 0.53 Mn, 0.055 S, 0.045 P, and a balance of Fe. HCl (analytical grade, 37%) and double distilled water were used to liquefy the HCl to produce the strong solution (2 M HCl). The allyl rhodanine azodye derivatives that were used in this paper and whose structures are presented in Table 1 were made in the lab by progressively incorporating 0.01 mol of  $\text{NaNO}_3$  into a hydrochloric acid solution of p-derivatives aniline with activation, and putting the resulting combination in an ice bath for about 20 minutes [29-31]. Step-by-step, with vigorous stirring, the obtained diazonium chloride solutions were added to a 0.01 mol cold solution of 3-allyl-4-hydroxythiazole-2(3H)-thione in 20 ml pyridine. The reaction mixture was agitated until it fully linked. The precipitate solid from the ethanol was nominated, water washed, dehydrated, and crystallized before being drained over anhydrous  $\text{CaCl}_2$ .

#### Methods

##### Tests for mass reduction

Using different grades of paper emery, acetone, bi-distilled water, and filter papers, rectangular C-steel coins with spacing of  $2.0 \times 2.0 \times 0.2$  cm were pounded. The coins were weighed carefully and then immersed in 100 cc of a 2 M hydrochloric acid solution at  $30^\circ\text{C}$  with no addition of inhibitors. The C-steel coins were taken out of each of the various submerge times, cleaned with bi-distilled water, left to dry, and then weighted once more. Eq. (1) uses the value of weight loss to get the frequency of oxidation (R) in  $\text{mmy}^{-1}$ :

$$R = (8.75 \times \text{mass reduction in gram} \times 10^4) / \text{DAT} \quad (1)$$

where T = time exposure in hr, A = focus region in  $\text{cm}^2$  and D = density of iron ion  $\text{g cm}^{-3}$ . Protection effectiveness (% IE) and ( $\theta$ ) were measured from Eq. (2):

$$\% \text{IE} = \theta \times 100 = [(R^* - R) / R^*] \times 100 \quad (2)$$

where  $R^*$  and  $R_a$  are the frequencies of C-steel corrosion without and with inhibitor, severally.

**Table 1:** Molecular structures, names, Molecular weights and Molecular formulas of investigated compounds.

Compound No.	Structure	Name	Mol. Wt. / Mol. Formula
(1)		(E)-3-Allyl-5-((4-methoxyphenyl) diazenyl)-2-thioxothiazolidin-4-one	307 $\text{C}_{13}\text{H}_{13}\text{N}_3\text{O}_2\text{S}_2$
(2)		(E)-3-Allyl-5-((4-methylphenyl) diazenyl)-2-thioxothiazolidin-4-one	291 / $\text{C}_{13}\text{H}_{13}\text{N}_3\text{OS}_2$
(3)		(E)-3-Allyl-5-((4-chlorophenyl) diazenyl)-2-thioxothiazolidin-4-one	311.5 / $\text{C}_{12}\text{H}_{10}\text{ClN}_3\text{OS}_2$

#### Electrochemical methods

Gamry potentiostat/galvanostat/ZRA (model PCI300/4) was used to simulate a three-electrode thermostatic cell assembly and perform electrochemical calculations. A saturated calomel electrode (SCE) and platinum foil were continuously utilized as reference and counter electrodes. The  $1 \times 1$  cm C-steel electrodes were fused to a copper wire used for electrical connectivity on one side. The electrodes were beaten, cleaned, and tested for mass loss. The temperature for all techniques was  $(30 \pm 1^\circ\text{C})$ . After reaching steady state (30 min), the potentiodynamic diagrams were recorded within the

range of  $\sim 5$  to 500 mV and scan rate  $1 \text{ mV S}^{-1}$ , and (OCP) was detected after placing the electrode in the solution test for 15 min. % IE and  $\theta$  were computed using Eq. (3):

$$\text{IE \%} = 100 \times \theta = 100 \times [1 - (i_{\text{corr}}^0 / i_{\text{corr}})] \quad (3)$$

Where  $i_{\text{corr}}^0$  and  $i_{\text{corr}}$ , respectively, represent the density of the corrosion currents of both uninhibited and inhibited

solution. The EIS and EFM tests, which were carried out using a Gamry framework system based on the ESA400, utilized the identical behaviors as before. Gamry applications comprise the programmers EFM140 to conduct EFM calculations and EIS300 for EIS tests; a computer was used for data summing. Plotting, graphing, and value fitting were done using Echem Analyst 5.5 software. EIS measurements were conducted using ac signals at different corrosion potentials, with a 5 mV magnitude and frequencies ranging 100 kHz and 10 mHz. EFM uses two frequencies, 2 and 5 Hz, to operate. 1 Hz served as the frequency base

#### SEM-EDX tests

Coins were immersed in 2 M hydrochloric acid for a period of three days without and with a high dose of allyl rhodanine azodye derivatives to prepare the surface of C-steel (1-3), followed by mechanically pounding with emery up to 1200 grit size instead of using paper. Following this time of inundation, the coins were carefully cleaned with distilled water, properly dried, and then placed into the spectrometer. The alloy-corroded edges were inspected utilizing a Philips X-ray diffractometer (pw-1390) and a Cu-tube (CuKa,  $\lambda = 1.54051$ ). (SEM, JOEL, JSM-T20, Japan).

#### Results and discussion

##### Mass reduction method

Figure 1 displays the time-mass reduction charts for C-steel corrosion in 2 M acid in the presence and absence of various chemical (1) dosages at  $30 \pm 1$  °C. The same figures were created for other compounds as well; however, they are not displayed. The results of Table 2 demonstrate that as the inhibitor dose is increased from  $1 \times 10^{-6}$  to  $11 \times 10^{-6}$  M, the effectiveness of protection increases. At  $11 \times 10^{-6}$  M, the best (% IE) was discovered. Since compound (3) provides the minimum (% IE), % IE tends to decrease in the order listed below: (1) > (2) > (3).

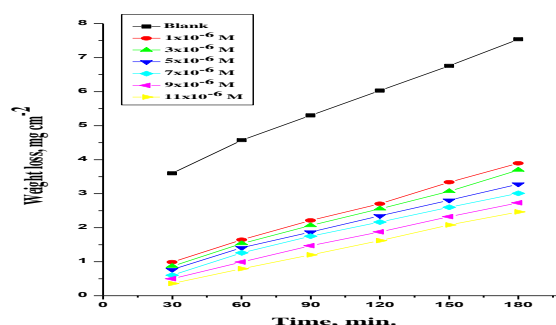


**Fig. 1.** Time – mass reduction curves for C-steel dissolution in 2 M HCl without and with unlike dose of inhibitor (1) at  $30 \pm 1$  °C.

**Table 2:** Variation of %IE of unlike compounds with their molar concentrations from mass loss method at 60 min immersion in acidic medium at  $30 \pm 1$ °C.

Conc. (M)	Inhibition efficiency (%IE)		
	Compound (1)	Compound (2)	Compound (3)
$1 \times 10^{-6}$	64.0	62.4	58.6
$3 \times 10^{-6}$	66.5	66.0	63.9
$5 \times 10^{-6}$	69.8	69.5	69.0
$7 \times 10^{-6}$	78.5	72.4	72.0
$9 \times 10^{-6}$	79.3	75.0	74.9
$11 \times 10^{-6}$	82.6	79.7	79.3

#### Adsorption isotherm

The interplay among the molecules that adsorb themselves to the surface of the electrode and the adsorption isotherm sheds significant light on corrosion prevention mechanisms [32]. Adsorption Temkin isotherm was best obtained for the outcome data in this work. Equation 4 produces the isotherm:

$$\theta = 2.303/a \log K_{\text{ads}} + 2.303/a \log C \quad (4)$$

where  $K_{\text{ads}}$  = equilibrium adsorption constant and  $C$  = dose of inhibitor. The plot of  $\log C$  against  $\theta$  was relation straight (given in Figure 2). The  $K_{\text{ads}}$  can be calculated using the intercept.

Also, the following equation can yield  $\Delta G_{\text{ads}}^{\circ}$ :

$$\log K_{\text{ads}} = -\log 55.5 - \Delta G_{\text{ads}}^{\circ} / 2.303RT \quad (5)$$

where  $T$  is the absolute temperature [33,34],  $R$  is the gas universal constant, and 55.5 is the mole/liter dose of water in solution [33]. As indicated in Table 3, the data for  $K_{\text{ads}}$  were attendance at the parallel run to the %IE [ $K(1) > K(2) > K(3)$ ]. Due to the creation of structural elements on the alloy surface, this result inverts the improvement in capability [35].

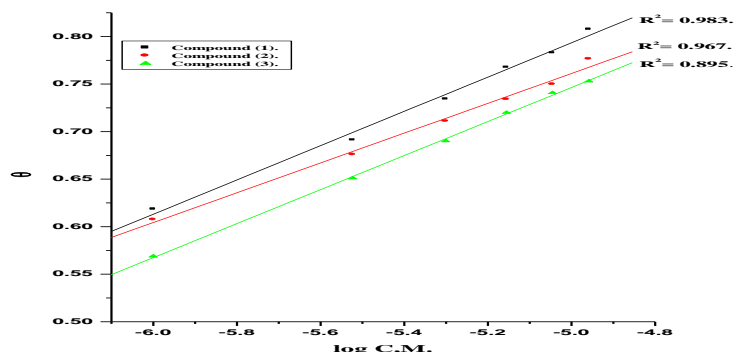


**Fig. 2.** Curve fitting of corrosion data for C-steel in 2 M HCl in presence of various dose of inhibitors to the Temkin isotherm at  $30 \pm 0.1$  °C.

**Table 3:** Inhibitor binding constant ( $K_{ads}$ ), ( $\Delta G_{ads}$ ) and later interaction parameter ( $a$ ) for inhibitors at  $30 \pm 0.1$  °C.

Inhibitor	Temkin isotherm		
	$a$	$K_{ads}$ ( $M^{-1}$ )	$-\Delta G_{ads}$ ( $kJ\ mol^{-1}$ )
Compound (1)	13.95	1.32	10.83
Compound (2)	13.91	1.27	10.71
Compound (3)	8.71	1.26	10.70

### Temperature influence

Measurements of the Arrhenius kind show that the activation energies ( $E_a^*$ ) for the presence of C-steel corrosion and absence of different doses of allyl rhodanine azodye derivatives (1-3) were as follows [36]:

$$\log k = \log A - E_a^*/2.303RT \quad (6)$$

The corrosion activation energy is denoted by the symbol  $E_a^*$ , whereas the constant rate is denoted by  $k$ , the pre-exponential factor by  $A$ , the absolute temperature by  $T$ , and the constant gas universal by  $R$ . The Arrhenius curves of  $1/T$  vs.  $\log k$  for an alloy in 2 M hydrochloric acid are shown in Figure 3 with and without various inhibitor (1) dosages. The difference is in a straight line. The slope of these lines was used to calculate the data for  $E_a^*$ , which are shown in Table 4. The energy barrier against corrosion improved as a result of the increase in  $E_a^*$  caused by the addition of inhibitor doses (1-3). Because the activation energy of the corrosion process is greater than  $20\ kJ\ mol^{-1}$ , the entire corrosion process is accurately carried out by surface reaction [37]. The performance of the transition state equation (7) was used to determine ( $\Delta H^*$ ,  $\Delta S^*$ ) for corrosion of carbon steel in an acidic media:

$$k = (TR/Nh) e^{(\Delta S^*/R)} e^{(-\Delta H^*/RT)} \quad (7)$$

where  $h$  is Planck's constant and  $N$  is Avogadro's number. Figure 4 shows linier lines for the liquefaction of C-steel in 2 M hydrochloric acid with and without inhibitor dose (1) generated from a plot of  $1/T$  against  $\log k/T$ .

The lines slopes =  $-\Delta H^*/2.303R$  and the intercept =  $\log RT/Nh + (\Delta S^*/2.303R)$  are shown in Table 4 together with the data for  $\Delta H^*$  and  $\Delta S^*$ . Based on these findings, the tested composite's presence increased  $E_a^*$  values, which in turn reduced the rate of C-steel corrosion. The explanation for these outcomes is that the investigated composites function as inhibitors by preventing charge transfer by their adsorption on alloy surfaces, hence accelerating the liquefaction of C-steel. The endothermic type for the liquefaction of C-steel is inverted by the +ve sign of the enthalpies.

The development of both a simple hydrogen response and a gaseous reaction is required for the corrosion process a reduced overall reaction volume because all  $E_a^*$  data are greater than comparable  $\Delta H^*$  data [38]. As a result of the examined compounds' greater and negative  $\Delta S^*$  attendance and absence data, the activated complex associates rather than dissociates during the rate-determining phase, which lowers the level of disordering [39,40].

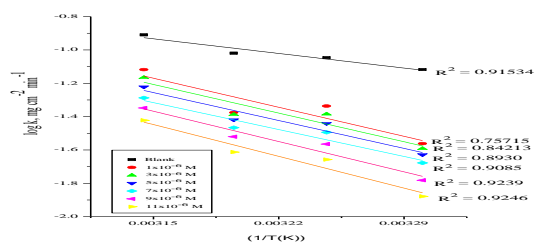


**Fig. 3.** Arrhenius plots (log  $k$  vs.  $1/T$ ) for C-steel in 2 M HCl in absence and presence of different doses of inhibitor (1).

#### Tafel polarization methods

To discover more about the kinetics of the anodic and cathodic reactions, polarization tests have been conducted. Figure 5 shows the alloy electrode's polarization behavior in an acidic solution without the presence of an opposing compound dosage (1). The cathodic response was shown in Figure 5 to be more protecting than the anodic reaction when the investigated allyl rhodanine azodye derivatives (1-3) were added. The %IE increased as the inhibitor dose rose. This shows how adding allyl rhodanine azodye derivatives (1-3) reduced anodic C-steel liquefaction and prevented the cathodic reactions. In order to act as mixed type inhibitors, the studied allyl rhodanine azodye derivatives (1-3) are used.

Table 5 displays the results, and it is evident that the addition of inhibitors has resulted in a drop in the current corrosion density and that %IE increases as inhibitor dose increases. The %IEp was measured in the manner described below:

$$\%IE_p = [i_{\text{corr}}^0 - i_{\text{corr}}] / i_{\text{corr}}^0 \times 100 \quad (8)$$

where  $i_{\text{corr}}$  and  $i_{\text{corr}}^0$  are the density of the corrosion currents that are inhibited and uninhibited, respectively.

Adsorbed inhibitors simply block the active centre for both cathodic and anodic processes, according to Table 5's findings. In another way, only a portion of the surface is rendered inactive by the inhibitors adsorbed in relation to the corrosive solution and do not affect the C-steel corrosion mechanism [41,42]. These composites' protective effectiveness follows the rule: (1) > (2) > (3). According to evidence from mass reduction techniques, this pattern is caused by a free pair of electrons in the molecular structure's alternate position, electrons on aromatic nuclei, a N atom, and another inversion. As a result, the ability to inhibit 2 M hydrochloric acid increases from (1) to (2) to (3).

Adsorbed inhibitors simply block the active centre for both cathodic and anodic processes, according to Table 5's findings. In another way, only a portion of the surface is rendered inactive by the inhibitors adsorbed in relation to the corrosive solution and do not affect the C-steel corrosion mechanism [41,42]. These composites' protective effectiveness follows the rule: (1) > (2) > (3). According to evidence from mass reduction techniques, This pattern is caused by a free pair of electrons in the molecular structure's alternate position, electrons on aromatic nuclei, a N atom, and another inversion. As a result, the ability to inhibit 2 M hydrochloric acid increases from (1) to (2) to (3).

**Table 4:** Thermodynamic parameters for the liquefaction of C-steel in 2 M hydrochloric acid attendance and lack of unlike dose of allyl rhodanine azodye derivatives (1-3).

Inhibitor	Conc. (M)	$E_a^+$ (kJ mol <sup>-1</sup> )	$\Delta H^+$ (kJ mol <sup>-1</sup> )	$-\Delta S^+$ (J mol <sup>-1</sup> K <sup>-1</sup> )
Blank	Blank	24.01	21.42	195.76
	1x10 <sup>-6</sup>	47.66	45.06	125.82
	3x10 <sup>-6</sup>	47.02	45.42	128.53
	5x10 <sup>-6</sup>	47.80	46.20	133.31
	7x10 <sup>-6</sup>	48.19	46.58	139.56
	9x10 <sup>-6</sup>	49.74	47.14	143.05
Compound (1)	11x10 <sup>-6</sup>	52.14	49.54	147.02
	1x10 <sup>-6</sup>	46.23	45.02	146.73
	3x10 <sup>-6</sup>	46.78	45.21	146.76
	5x10 <sup>-6</sup>	47.35	45.38	146.83
	7x10 <sup>-6</sup>	48.07	46.19	183.58
	9x10 <sup>-6</sup>	49.62	47.06	188.96
Compound (2)	11x10 <sup>-6</sup>	51.90	49.31	191.46
	1x10 <sup>-6</sup>	45.78	44.63	153.10
	3x10 <sup>-6</sup>	45.92	44.76	154.61
	5x10 <sup>-6</sup>	46.63	45.06	146.92
	7x10 <sup>-6</sup>	47.23	45.87	186.32
	9x10 <sup>-6</sup>	47.78	46.91	189.99
Compound (3)	11x10 <sup>-6</sup>	48.29	48.65	194.70

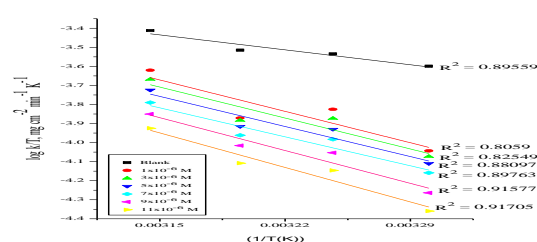


**Fig. 4.** Transition state plots (log  $k/T$  vs.  $1/T$ ) for C-steel in 2 M HCl in absence and presence of unlike concentration of inhibitor

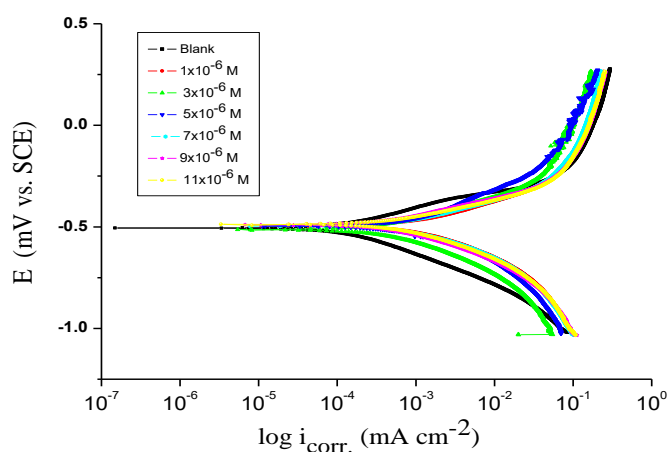


**Fig. 5.** Potentiodynamic polarization curves for the corrosion of C-steel in 2 M HCl attendance and lack of unlike dose of compound (1) at  $30 \pm 0.1$  °C.

### EIS techniques

EIS is a strength test [43–47]. Figure 6 displays, the presence and lack of enhancing doses of the tested allyl rhodanine azodye compounds at open-circuit potential using Nyquist (a) and Bode (b) curves. With the addition of allyl rhodanine azodye derivatives, the capacitive loop's surface area increased, demonstrating the gradual formation of a barrier on the alloy surface. The capacitive loop in Figure 6(a) increases in size at constant inhibitor dose when the orders of (1) > (2) > (3) are used, indicating that derivatives have the greatest protective effect (1).

In contrast to what the EIS theory predicts, the Nyquist curves do not result in perfect semicircles. Stepwise imputed to the dispersion frequency was the declination from the semicircle ideal [48]. Given a single reaction charge transfer, The EIS spectra of the organic appendages were measured using the equivalent circuit depicted in Figure 7, and the results were in good agreement with those of our experiments. To achieve a better match, the CPE is embedded the electrical equivalent of a dual-layer pure capacitor [49]. Equation (9) measures the double layer capacitance, Cdl:

$$C_{dl} = Y_o \omega^{n-1} / \sin [n (\pi/2)] \quad (9)$$

$Y_o$  is the CPE's magnitude,  $2\pi f_{max}$  is the imaginary component's highest frequency of the impedance, is two times  $f_{max}$ , and  $n$  is used precisely between 0.50 and 1.0.

After approving the Nyquist curve plot, it is observed that the diagrams are almost entirely capacitive; indicating that the corrosion mechanism was a widely used instruction for charge transfer [50–52]. The majority of plots have relatively similar shapes including all solutions (at various flooding times, both with and without inhibitors), which results in no difference in the corrosion process [53]. The data of  $R_{ct}$  increase with increasing the inhibitor dose and thus given increase in IE, which is equivalent to the outcome of mass reduction, according to EIS value (Table 6) With the presence of an inhibitor, the  $R_{ct}$  data in an acidic medium increases. Double layer capacitance statistics are also reduced to their greatest extent when an inhibitor is present, and the lower data for CPE follow the same rules as those for  $i_{corr}$  in this study. Organic derivatives, which have a lower local dielectric constant and/or a thicker double layer, protect C-steel from corrosion caused by metal/acid adsorption [54,55]. The EIS crucial are to follow the metal's corrosion habits over a continuous period of time. The charge transfer resistance value from equation (10) was used to calculate the percentage of IE [56]:

$$\% IE_{EIS} = 100 \times [1 - (R_{ct}^o / R_{ct})] \quad (10)$$

where the resistance to charge transport data participation and lack of inhibitor, respectively, are  $R_{ct}^o$  and  $R_{ct}$ , respectively. Without any previous knowledge of Tafel slopes, EFM is non-destructive corrosion analysis methodology that can quickly measure the current corrosion data. These significant EFM tests make it a viable choice for online calculations of corrosion [57]. The components of causation that serve as an interior examination of the accuracy of EFM calculation. The frequency range's current is used to calculate the causality factors CF-2 and CF-3. The EFM spectrum of C-steel with 2 M HCl solution at various chemical concentrations are shown in Figure 8 (1). Plots similar to those for other compounds were presented (not shown). Background noise is noticeably lower than the ocular harmonic and intermodulation band that is experienced. EFM values were handled using the "activation" theory and full control diffusion of the cathodic process. As summing that the polarization of the electrode's operation has no effect on the potential for corrosion, triple non-linear equations in a sequence has been developed for the second case [58]. The current corrosion density ( $i_{corr}$ ), (c and a), and the greater peaks (CF-2 and CF-3). The electrochemistry parameters are listed in Table 7.

The value in Table 7 clearly shows that any specified composite may be added at a specific dose to an acidic medium reduced  $i_{corr}$  and caused these composites to adsorb to an alloy in 2 M hydrochloric acid to stop it from corroding. The calculated data are flawless and of the highest quality because the causes of causation discovered under dissimilar testing are almost identical to conceptual information (2 and 3). By increasing the inhibitor dose as shown in equation (11):

$$\% IE_{EFM} = [1 - (i_{corr} / i_{corr}^o)] \times 100 \quad (11)$$

where the corrosion currents' present and absent inhibitors' intensities are, respectively,  $i_{ocorr}$  and  $i_{corr}$ . According to these tests, protection is sufficient in the following order: (1) > (2) > (3).

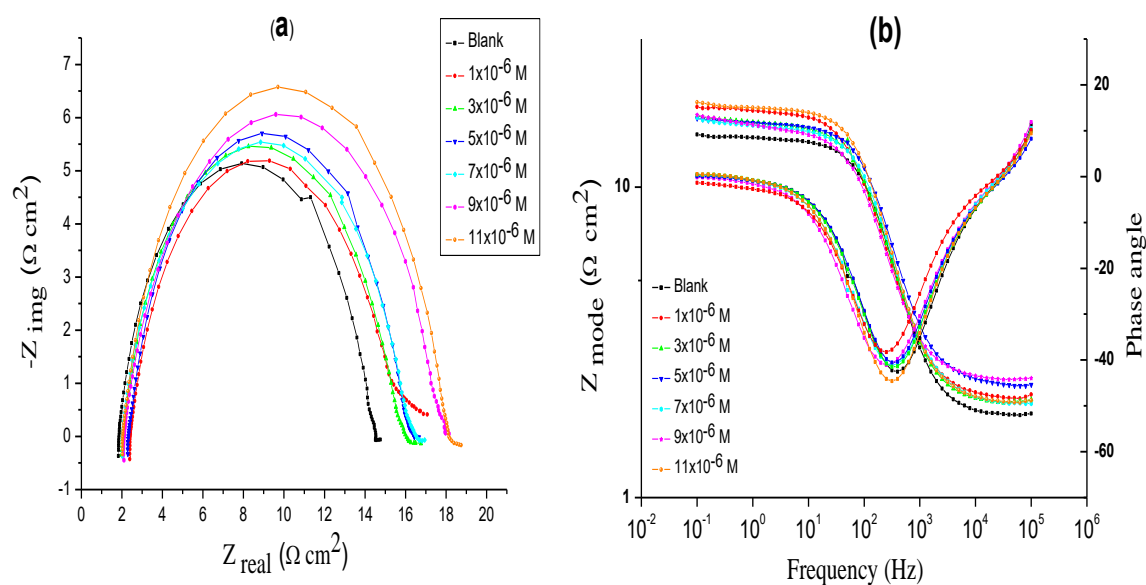


**Fig. 6.** EIS Nyquist plots (a) and Bode plots (b) for C-steel surface in 2 M HCl attendance and lack of unlike dose of compound (1) at  $30 \pm 0.1$  °C.

**Table 5:** Effect of dose of the investigated allyl rhodanine azodye derivatives (1-3) on the free corrosion potential ( $E_{corr}$ ), ( $i_{corr}$ ), ( $\beta_a$  &  $\beta_c$ ), ( $\theta$ ) and (% IE) for C-steel in 2 M HCl at  $30 \pm 0.1$  °C.

Compound	Conc. (M)	$-E_{corr} \times 10^{-3}$ (mV vs. SCE)	$i_{corr} \times 10^{-5}$ ( $\mu\text{A cm}^{-2}$ )	$\beta_a \times 10^{-3}$ (mV dec $^{-1}$ )	$\beta_c \times 10^{-3}$ (mV dec $^{-1}$ )	$\theta$	% IE
	Blank	505	8.99	79.5	109.3	----	-----
(1)	$1 \times 10^{-6}$	487	2.15	40.6	47.2	0.760	76.0
	$3 \times 10^{-6}$	483	1.95	102.5	108.4	0.783	78.3
	$5 \times 10^{-6}$	496	1.61	36.6	49.9	0.820	82.0
	$7 \times 10^{-6}$	487	1.56	23.3	28.0	0.826	82.6
	$9 \times 10^{-6}$	482	1.53	18.6	19.9	0.829	82.9
	$11 \times 10^{-6}$	474	1.23	17.6	21.9	0.863	86.3
(2)	$1 \times 10^{-6}$	499	3.45	25.0	28.9	0.616	61.6
	$3 \times 10^{-6}$	492	3.29	17.2	14.5	0.634	63.4
	$5 \times 10^{-6}$	496	3.24	26.8	30.9	0.639	63.9
	$7 \times 10^{-6}$	491	2.92	25.5	25.3	0.675	67.5
	$9 \times 10^{-6}$	484	2.81	22.4	24.4	0.687	68.7
	$11 \times 10^{-6}$	489	2.75	23.4	28.5	0.694	69.4
(3)	$1 \times 10^{-6}$	496	7.04	92.7	114.7	0.216	21.6
	$3 \times 10^{-6}$	514	6.94	39.5	42.9	0.228	22.8
	$5 \times 10^{-6}$	496	6.70	133.2	133.5	0.254	25.4
	$7 \times 10^{-6}$	496	6.04	102.5	108.4	0.328	32.8
	$9 \times 10^{-6}$	489	4.02	95.3	116.2	0.552	55.2
	$11 \times 10^{-6}$	488	3.58	26.8	31.7	0.601	60.1

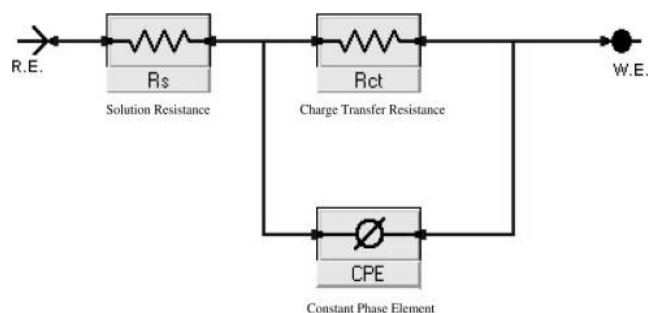


Fig. 7. Equivalent circuit model utilized to fit experimental EIS.

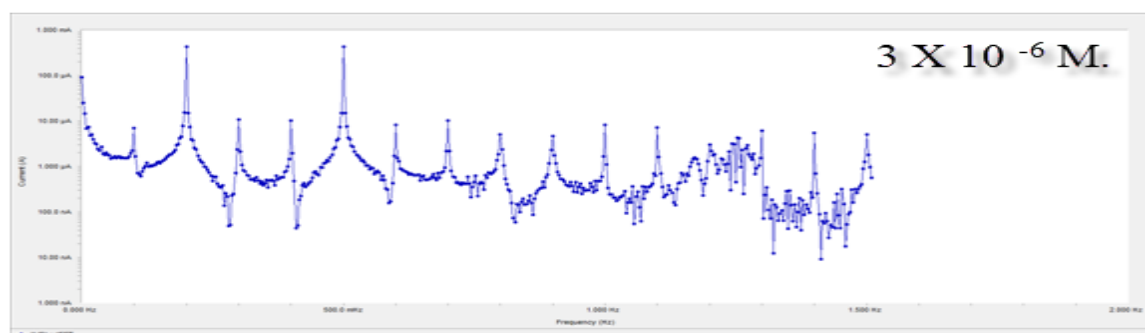
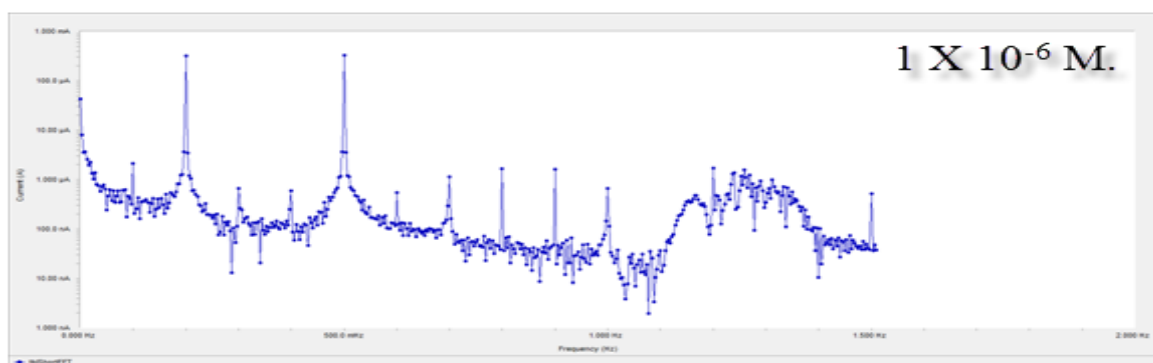
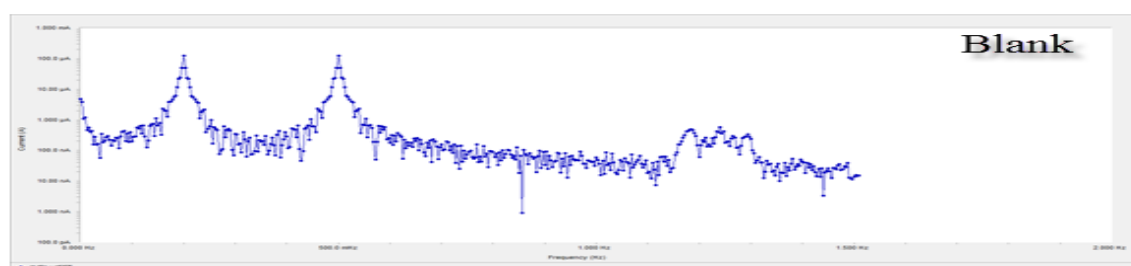
Table 6: Electrochemical kinetic parameters given by EIS method for C-steel in 2 M HCl without and with various dose of compounds (1-3) at  $30 \pm 0.1$  °C.

Inhibitors	Conc. (M)	$R_s$ ( $\Omega \text{ cm}^2$ )	$Y_o \times 10^{-4}$	$n \times 10^{-1}$	$R_{ct}$ ( $\Omega \text{ cm}^2$ )	$C_{dl} \times 10^{-4}$ ( $\mu\text{Fcm}^{-2}$ )
Compound (1)	Blank	1.849	2.38	8.79	12.57	1.07
	$1 \times 10^{-6}$	2.162	3.70	8.37	20.44	1.43
	$3 \times 10^{-6}$	2.235	4.64	8.27	21.38	1.77
	$5 \times 10^{-6}$	1.658	1.62	8.80	23.26	0.754
	$7 \times 10^{-6}$	11.09	2.89	8.29	28.71	1.07
	$9 \times 10^{-6}$	12.8	1.03	5.76	39.92	0.989
	$11 \times 10^{-6}$	1.752	2.16	8.48	84.18	1.05
	$1 \times 10^{-6}$	1.582	2.25	8.75	16.18	1.00
Compound (2)	$3 \times 10^{-6}$	2.093	3.32	8.52	16.58	1.35
	$5 \times 10^{-6}$	2.095	2.02	8.69	16.77	0.860
	$7 \times 10^{-6}$	2.491	3.74	8.35	18.08	1.40
	$9 \times 10^{-6}$	1.612	1.97	8.58	18.2	0.777
	$11 \times 10^{-6}$	2.038	3.21	8.68	19.74	1.48
Compound (3)	$1 \times 10^{-6}$	2.402	3.96	8.43	13.53	1.50
	$3 \times 10^{-6}$	2.032	2.66	8.62	13.79	1.08
	$5 \times 10^{-6}$	2.326	2.29	8.73	13.83	0.988
	$7 \times 10^{-6}$	2.026	2.94	8.58	14.23	1.18
	$9 \times 10^{-6}$	2.098	3.69	8.37	15.7	1.36
	$11 \times 10^{-6}$	2.047	2.29	8.80	16.04	1.07



**Table 7:** Electrochemical kinetic parameters obtained by EFM tests for C-steel in 2 M HCl without and with unlike dose of compounds (1-3) at  $30 \pm 0.1$  °C.

Inhibitors	Conc. (M)	$i_{corr}$ ( $\mu\text{A cm}^{-2}$ )	$\beta_a \times 10^{-3}$ ( $\text{mV dec}^{-1}$ )	$\beta_c \times 10^{-3}$ ( $\text{mV dec}^{-1}$ )	CF-2	CF-3	$\theta$	%IE
Compound (1)	Blank	812.2	40.9	43.1	1.92	2.85	-----	-----
	$1 \times 10^{-6}$	269.2	30.3	31.6	1.89	2.64	0.668	66.8
	$3 \times 10^{-6}$	269.0	28.7	33.9	2.03	3.01	0.669	66.9
	$5 \times 10^{-6}$	259.9	28.0	30.9	2.02	3.04	0.680	68.0
	$7 \times 10^{-6}$	253.6	27.0	29.7	2.04	3.33	0.687	68.7
	$9 \times 10^{-6}$	244.9	25.8	28.1	1.85	2.37	0.698	69.8
Compound (2)	$11 \times 10^{-6}$	136.3	78.4	29.6	2.09	2.94	0.832	83.2
	$1 \times 10^{-6}$	307.7	36.0	47.4	1.83	3.02	0.621	62.1
	$3 \times 10^{-6}$	304.7	35.8	38.2	1.93	2.98	0.624	62.4
	$5 \times 10^{-6}$	293.3	32.8	38.1	1.96	2.86	0.638	63.8
	$7 \times 10^{-6}$	292.5	33.0	37.2	1.68	2.76	0.639	63.9
Compound (3)	$9 \times 10^{-6}$	271.6	28.4	35.3	2.07	3.00	0.665	66.5
	$11 \times 10^{-6}$	271.5	30.5	32.2	1.76	2.56	0.6657	66.5
	$1 \times 10^{-6}$	767.7	156.9	43.1	1.97	3.03	0.0547	5.47
	$3 \times 10^{-6}$	714.9	100.0	152.8	2.02	2.97	0.119	11.9
	$5 \times 10^{-6}$	360.3	43.9	117.8	1.84	2.55	0.556	55.6
	$7 \times 10^{-6}$	353.9	42.4	48.5	2.03	2.96	0.564	56.4
	$9 \times 10^{-6}$	339.8	39.2	48.4	1.49	2.81	0.581	58.1
	$11 \times 10^{-6}$	326.2	39.4	41.5	2.07	3.06	0.598	59.8



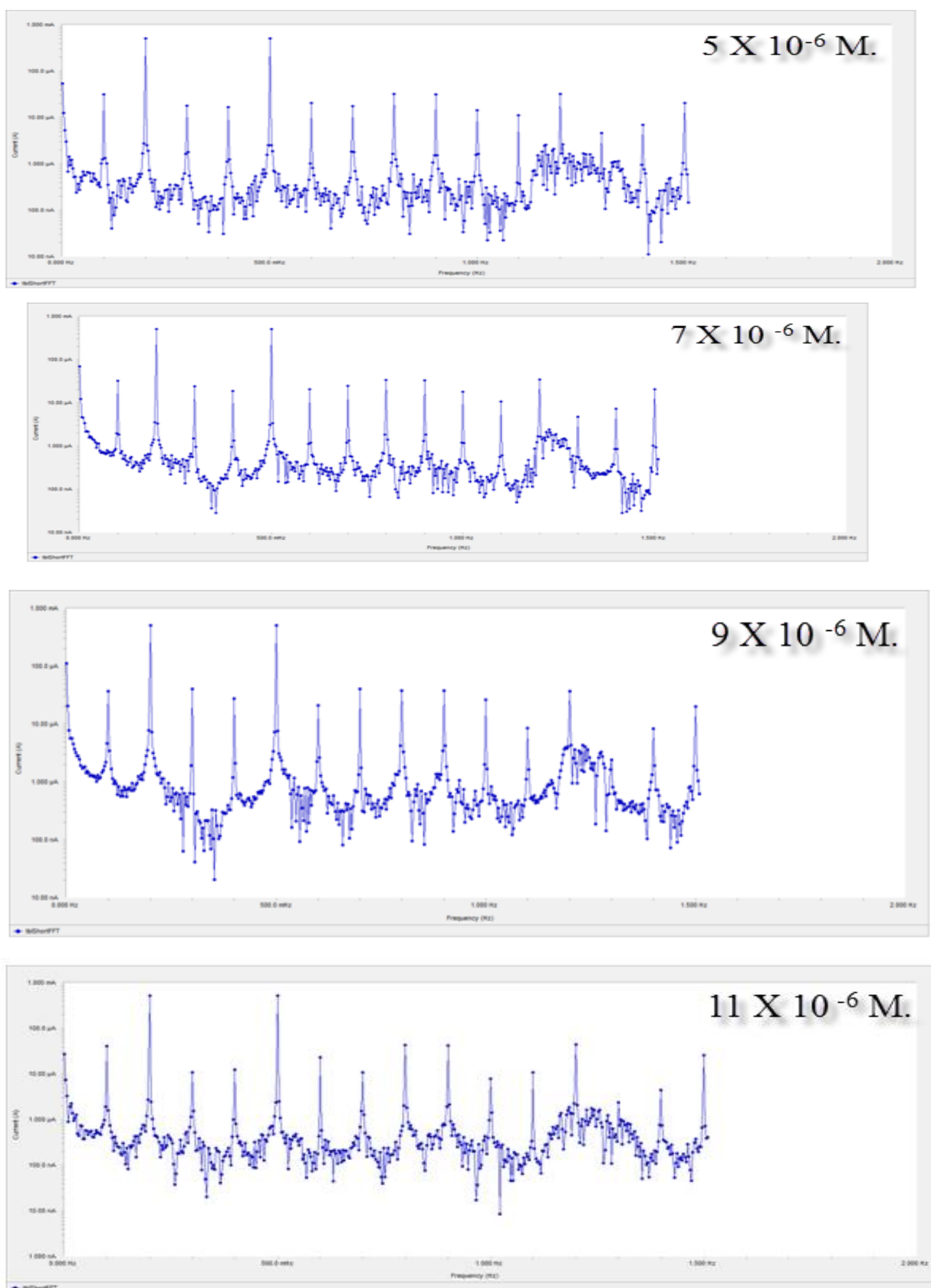


**Fig. 8.** EFM spectra for C-steel in 2 M HCl attendance and lack of unlike dose of compound (1) at  $30 \pm 0.1$  °C.

### SEM tests

After being submerged for three days, the micrography of alloy coins with and without  $11 \times 10^{-6}$  M allyl rhodanine azodye derivatives (1-3) is shown in Figure 9. For the blank sample, C-steel surfaces experience severe corrosion attack. It is important to emphasize that when the compound is present in the solution; the morphology of C-steel is extremely different from the previous one and has the softer of the coin surfaces. Due to the allyl rhodanine azodye derivatives (1-3) adhering to the integrating into the passive film to prevent the active centre from being visible on the C-steel surface, we observed alloy surface and the development of a randomly dispersed film across all of the material surface [59]. Or because inhibitor molecules are involved in the reaction with the C-steel sites, the contact between C-steel and hydrochloric acid is reduced, which subsequently prevents a positive inhibition effect.

### EDS tests

After three days of soaking in both unfettered and inhibited 2M HCl, the elements' presence on the C-steel surface was measured using the EDS spectra. Figure 10 depicts the study of the EDS results for the C-steel composition with just the acid and treatment inhibitor. Solely O and Fe were obtained from the EDS tests, causing the passive film to solely contain  $\text{Fe}_2\text{O}_3$ . Figure 10 depicts an EDS analysis of C-steel carried out in 2 M HCl with  $11 \times 10^{-6}$  M of allyl rhodanine azodye derivatives (1-3). The spectra shown in the lines below show that C is real (owing to the carbon atoms of allyl rhodanine azodye derivatives). These measurements revealed that the surface of the coins was covered in C and O atoms. Because the alloy surface exposed to uncontrolled HCl lacks signals from C and O, this layer is solely due to the inhibitor. It is evident that the spectra of C and O were obtained by adding Mn. Table 8 shows a similar elemental distribution.

**Table 8:** Surface composition (wt%) of C-steel after 3 days immersion in HCl without and with the perfect dose of the studied allyl rhodanine azodye derivatives (1-3).

(Mass %)	C	O	Al	Si	Cr	Mn	Fe	Tb
<b>Pure Sample</b>	6.78	---	0.29	0.28	0.22	0.47	87.53	4.43
<b>Blank</b>	10.48	13.40	0.30	0.22	0.18	0.41	70.90	4.11
<b>Compound (1)</b>	11.85	9.11	0.30	0.32	0.19	0.46	77.25	0.52
<b>Compound (2)</b>	11.41	6.94	0.26	0.24	0.20	0.43	74.38	6.41
<b>Compound (3)</b>	10.60	15.30	0.31	0.29	0.19	0.40	71.11	1.80

### Quantum calculations

Molecules of allyl rhodanine azodye derivatives' Mulliken charges and orbital graphs are shown in Figure 11. (1-3). Only the neutral forms were used in the theoretical analysis in order to gain further understanding of the experimental results. Table 9 contains measurements of quantum chemical indices, including the least energies molecular orbitals that aren't loaded ( $E_{\text{LUMO}}$ ), the greatest molecular orbitals' energies ( $E_{\text{HOMO}}$ ), and energy gap (E). Studies show that the more electrons are provided to the metal's vacant d orbital, the bigger or lower the -ve  $E_{\text{HOMO}}$  is associated to the inhibitor, and the more successfully corrosion is prevented. In addition, the lower the  $E_{\text{LUMO}}$ , the more readily electrons can be extracted from the alloy surface [60-64].

According to Table 9, the electron transfer between the molecule's HOMO and LUMO orbitals is made easier by the compound (3)'s adsorption on the alloy surface, which results in a higher %IE. This strengthens the presumption that compound (1) will penetrate more effectively on C-steel surface (3).

Additionally, the  $E_{\text{HOMO}}$  rise from compound (1) to compound (3) supports the transport process across the adsorbed layer, facilitating adsorption and inhibition. According to reports, ideal corrosion Organic molecules are the source of inhibitors, which not only remove electrons from the metal and give them to an alloy's vacant orbital. Experimental validation of these results is done using all quantum calculation parameters.

### Chemical composition and anti-corrosion measures

The corrosive effects of various allyl rhodanine azodye derivatives on carbon steel in a solution of 2 M hydrochloric acid (1-3) is determined by mass reduction, potentiodynamic anodic polarization tests, EIS and EFM tests. The dose, the type of metal, the surface conditions, and the method of the inhibitors' adsorption all affect how effective the protection is these inhibitors have the following observed corrosion benefits:

- There is a reducing in corrosion rate and current with an inhibitor dose rising.
- The difference in mass reduction with time that is linear.
- The Tafel lines change to expand the potential area.
- The desorption of the adsorbed inhibitor molecules takes place as corrosion protection decreases with rising temperature.
- The charge density and number of active devices affect the protection effectiveness.

It was discovered that the adsorption mode depends on the alloy's propensity for the ring system's -electron clouds. Iron and other metals with a higher affinity for aromatic molecules were shown to be able to adsorb benzene rings with a flat orientation. The examined inhibitors' %IE was reduced in the corrosive medium in the following order: (1) > (2) > (3).

In addition to increasing the electron density on the molecule, the presence of the *p*- $\text{OCH}_3$  group, which is an electron-donor with a -ve Hammett constant (= -0.27), also results in a bigger molecular size that can readily cover the surface,

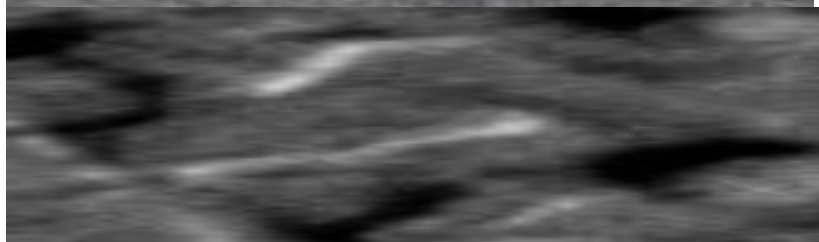
compound (1) has the best protective power. In terms of protective effectiveness, compound (2) comes in second. The presence of the electron-donor *p*-CH<sub>3</sub> group, which has a -ve Hammett constant ( $\sigma = -0.17$ ), is what causes this. Additionally, although less so than the *p*-OCH<sub>3</sub> group in the inhibitor (1), this group will raise the electron density on the molecule.

Because of the occurrence of the *p*-Cl group, which has a +ve Hammett constant ( $\sigma_{\text{Cl}} = +0.23$ ) and so decreases the molecule's electron density and hence the effectiveness of protection, compound (3) in % IE is the final.

Pure sample



Blank



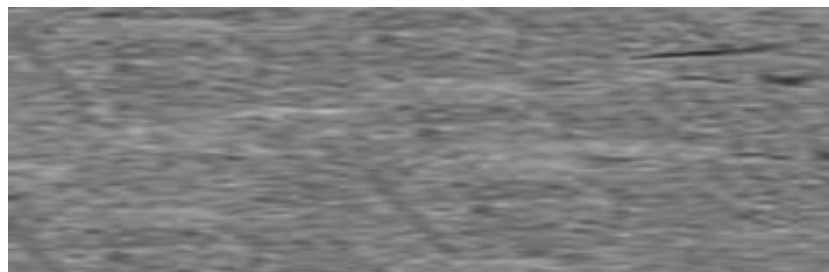
Compound (1)



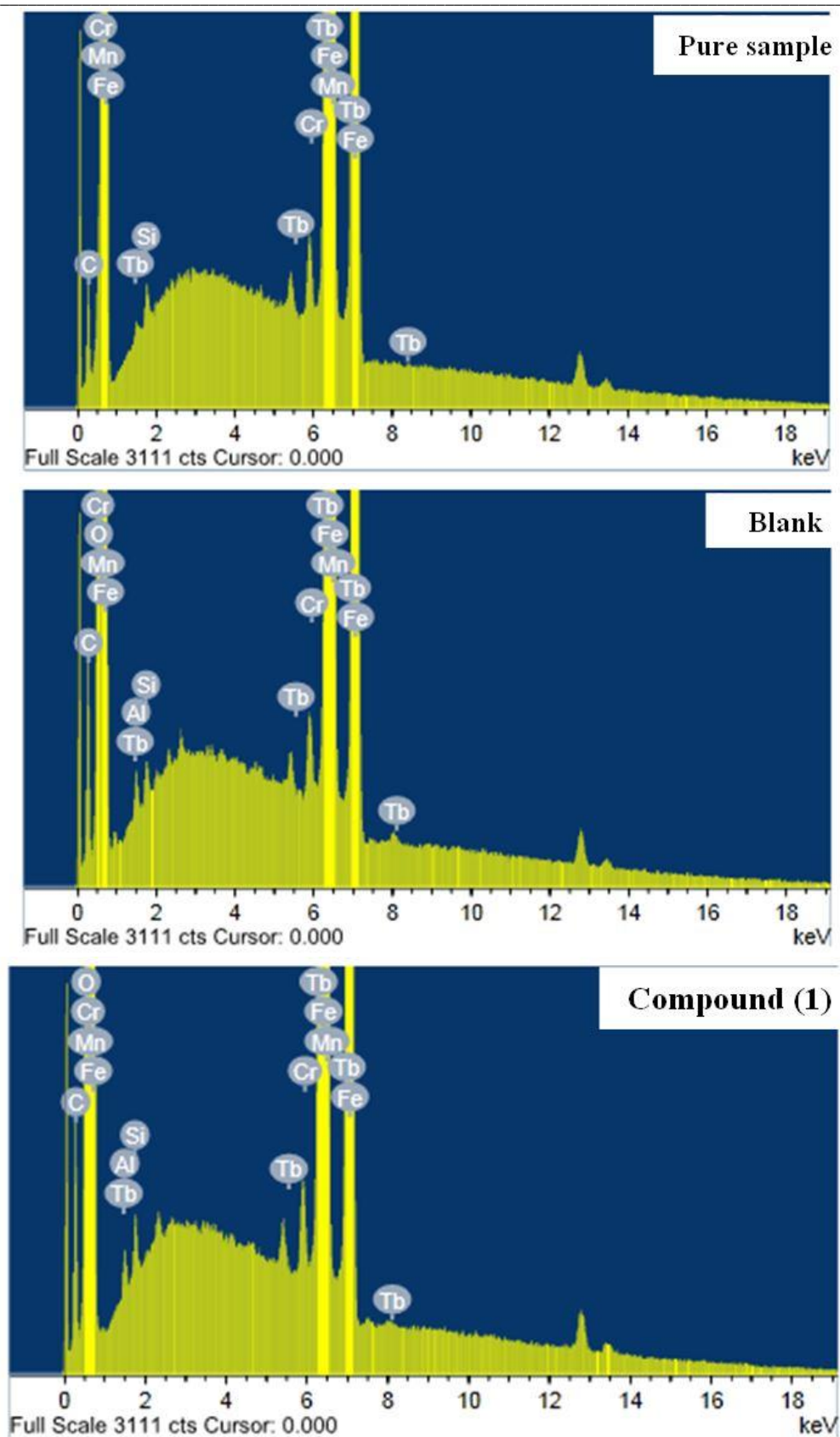
Compound (2)



Compound (3)



**Fig. 9.** SEM images of C-steel in 2 M HCl solution after immersion for 3 hrs without inhibitor and in presence of  $11 \times 10^{-6}$  M of allyl rhodanine azodye derivatives (1-3).



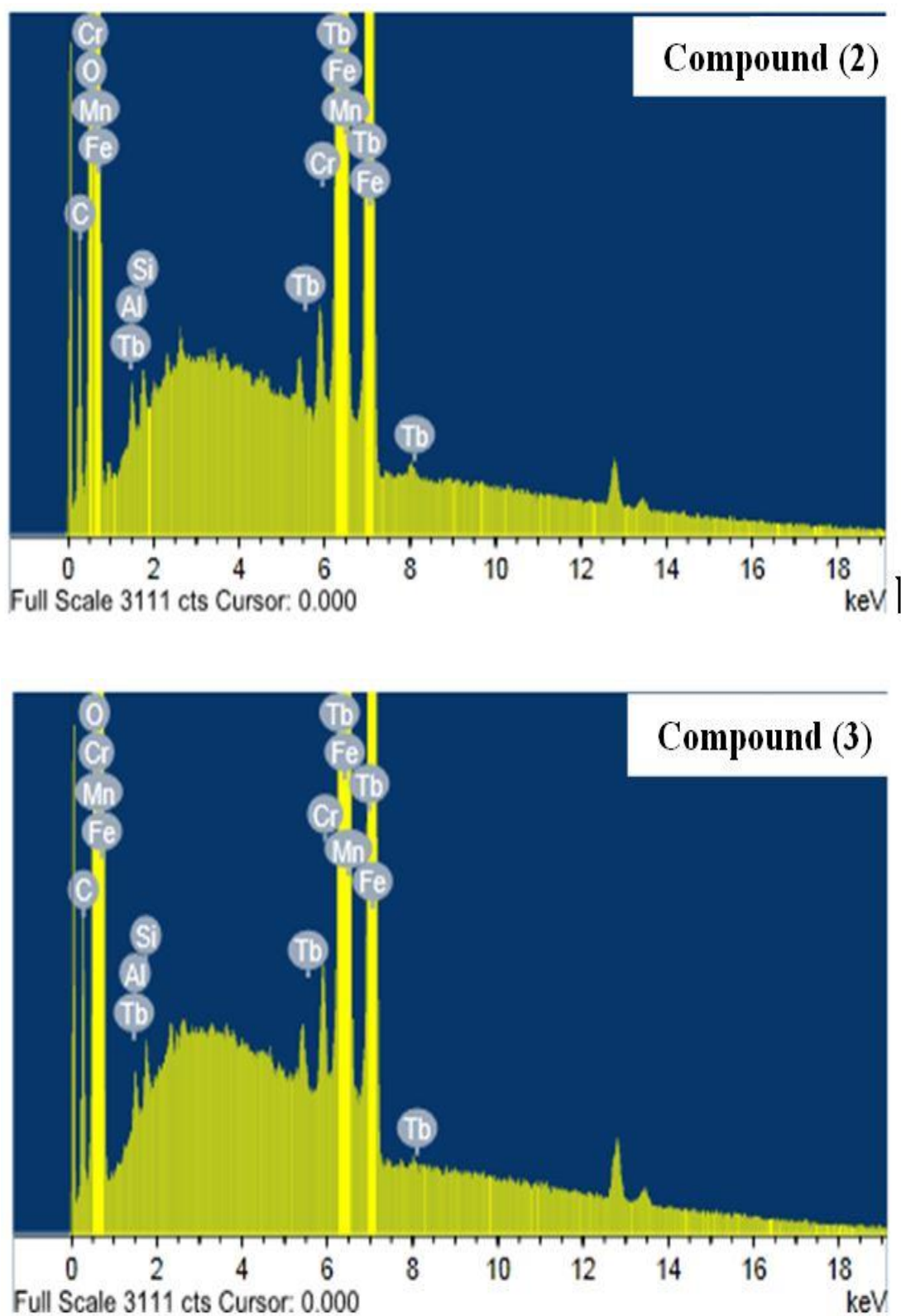


**Fig. 10.** EDS analysis of C-steel in 2 M HCl solution after immersion for 3hrs without inhibitor and in attendance of  $11 \times 10^{-6}$  M of allyl rhodanine azodye derivatives (1-3).



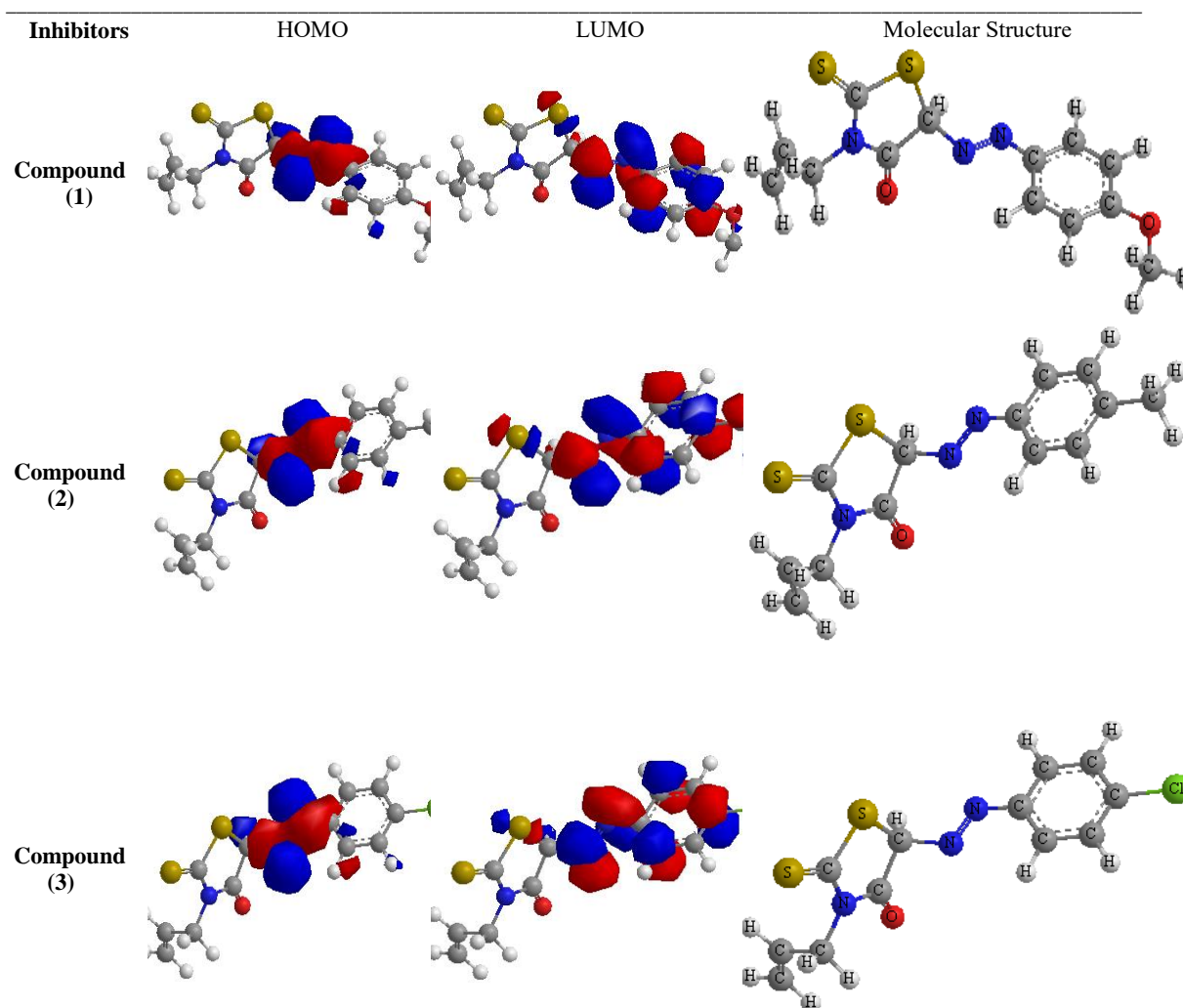


Fig. 11. Molecular orbital plots of investigated allyl rhodanine azodye derivatives (1-3).

Table 9: The calculated quantum chemical properties for investigated allyl rhodanine azodye derivatives (1-3).

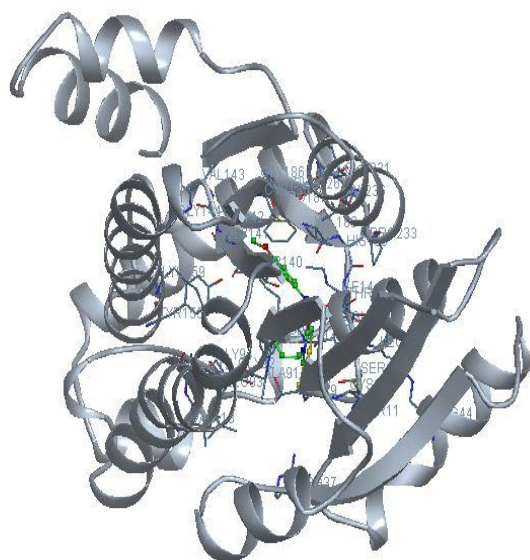
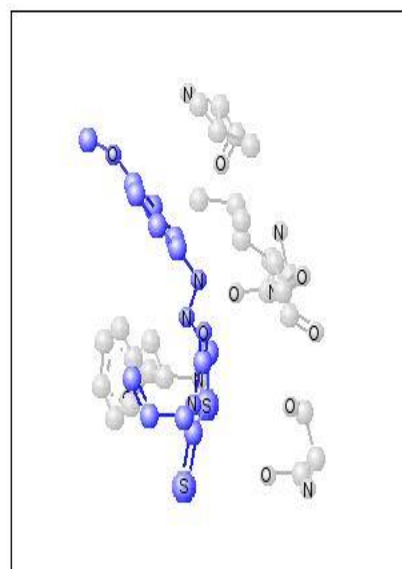
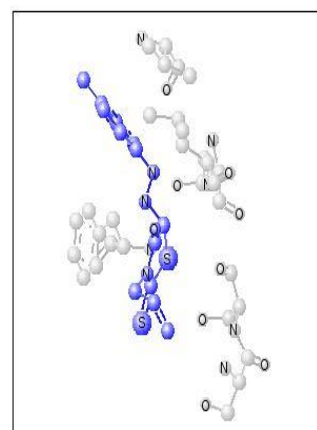
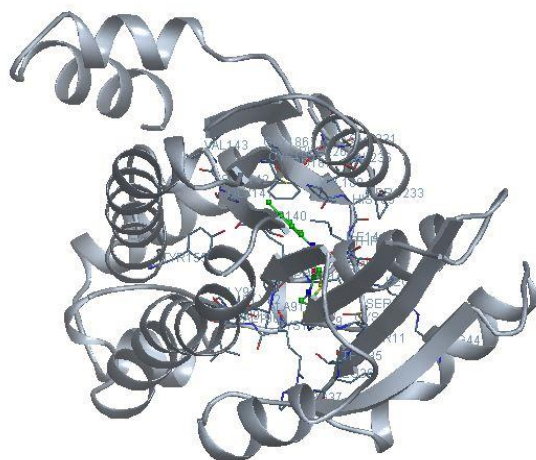
	Compound (1)	Compound (2)	Compound (3)
$-E_{\text{HOMO}}$ (eV)	3.345	3.336	3.330
$-E_{\text{LUMO}}$ (eV)	2.755	2.415	2.302
$\Delta E$ (eV)	0.590	0.921	1.028
$\eta$ (eV)	0.295	0.461	0.514
$\sigma$ (eV) <sup>-1</sup>	3.390	2.172	1.946
$-Pi$ (a.u)	3.050	2.876	2.816
$\chi$ (eV)	3.050	2.876	2.816
$S$ (eV) <sup>-1</sup>	1.695	1.086	0.973
$\omega$ (a.u)	15.767	8.978	7.714
$\Delta N_{\text{max}}$	10.339	6.244	5.479

### Molecular docking

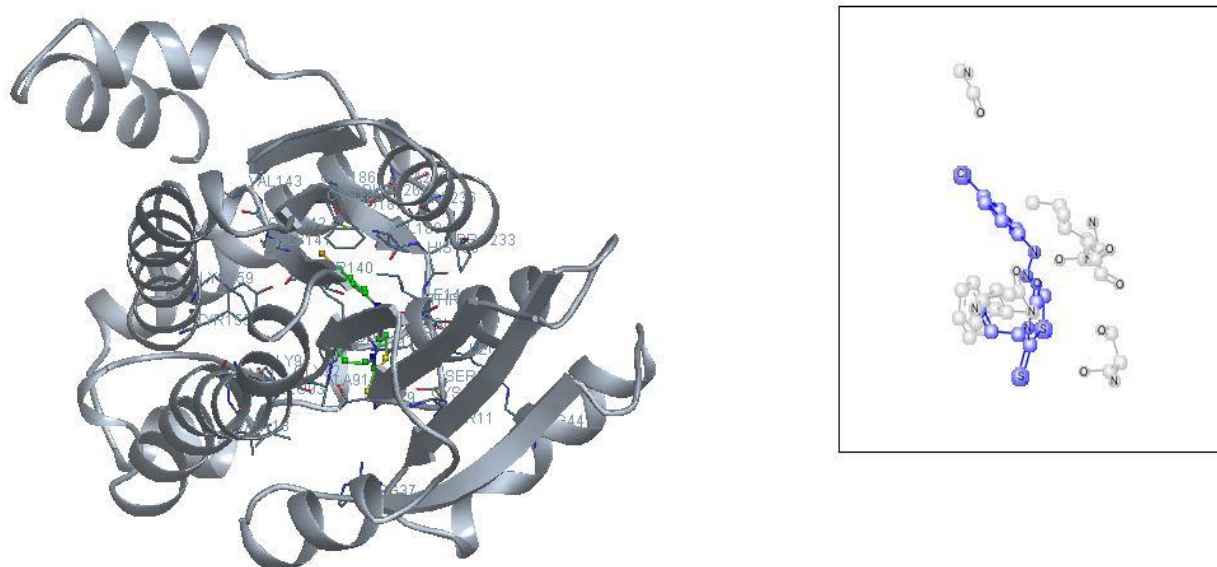
The report reveals a positive  $c$  contact among the breast cancer (3hb5) receptor and the allyl rhodanine azodye derivatives (1-3). Table 10 and Fig. 12 record the measured energy. Consistent with the findings of this investigation, the HB plot curve caused the allyl rhodanine azodye derivatives (1-3) to form hydrogen bond by linking to the two proteins. As seen on Fig. 13, the allyl rhodanine azodye derivatives (1-3) have decomposed connections values in kcal/mol (1-3) and 3hb5 receptor. When experimental  $K_i$  values were compared to AutoDock's estimated  $K_i$  values, when available, the observed efficiency is good [64,65] and the Gibbs free energy is negative [65-71]. On the basis of these findings, it is also possible to hypothesize that the allyl rhodanine azodye derivatives (1-3) and the 3hb5 receptor may interact. The 2D graphs for docking utilising allyl rhodanine azodye derivatives (1-3) are presented in Figure 14.

**Table 10:** Energy data given in docking calculations of allyl rhodanine azodye derivatives (1-3) with of breast cancer mutant 3hb5 receptor.

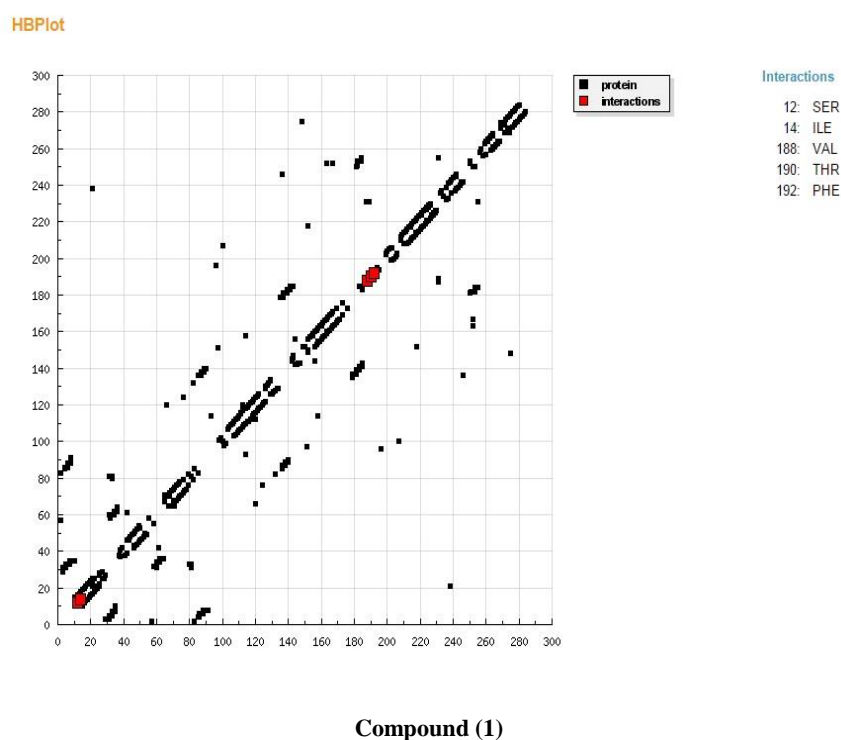
Compound	Est. free energy of binding (kcal/mol)	Est. inhibition constant ( $K_i$ ) ( $\mu$ M)	vdW+ bond+ desolve energy (kcal/mol)	Electrostatic Energy (kcal/mol)	Total intercooled Energy (kcal/mol)	Interact surface
<b>Compound (1)</b>	-7.08	6.51	-8.39	-0.07	-8.46	813.49
<b>Compound (2)</b>	-7.53	3.04	-8.64	-0.02	-8.66	805.79
<b>Compound (3)</b>	-7.97	1.44	-9.09	-0.04	-9.13	792.20

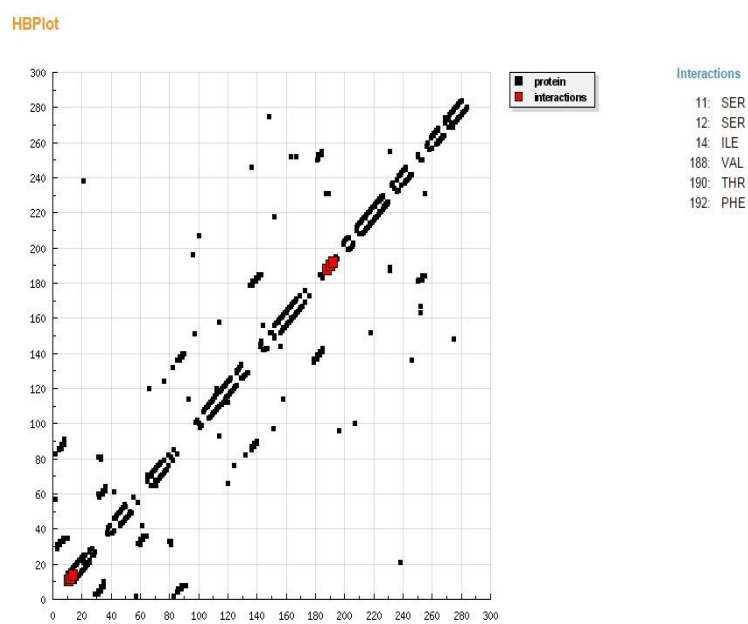
**Compound (1)****(B)****Compound (2)****Compound (3)**



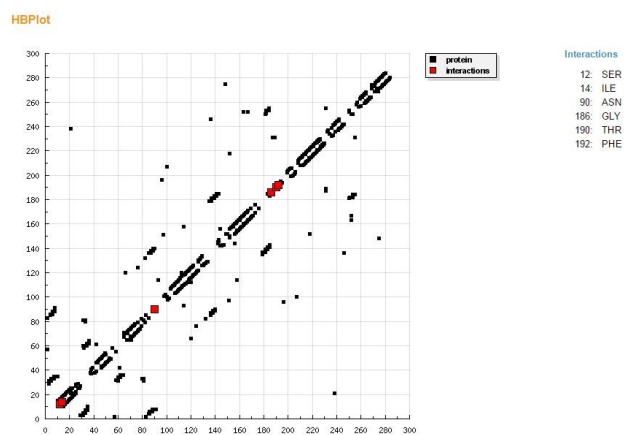


**Fig. 12.** The allyl rhodanine azodye derivatives (1-3) (green in (A) and blue in (B)) in interaction with breast cancer mutant 3hb5 receptor. (For interpretation of the references to colour in this figure legend, the reader is referred to the web version of this article).





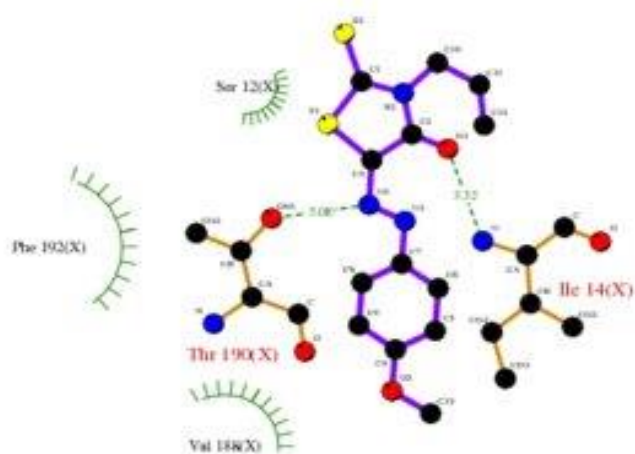
Compound (2)






Compound (3)


**Fig. 13.** HB plot of interaction between allyl rhodanine azodye derivatives (1-3) with receptor of breast cancer mutant 3hb5.

## Compound (1)



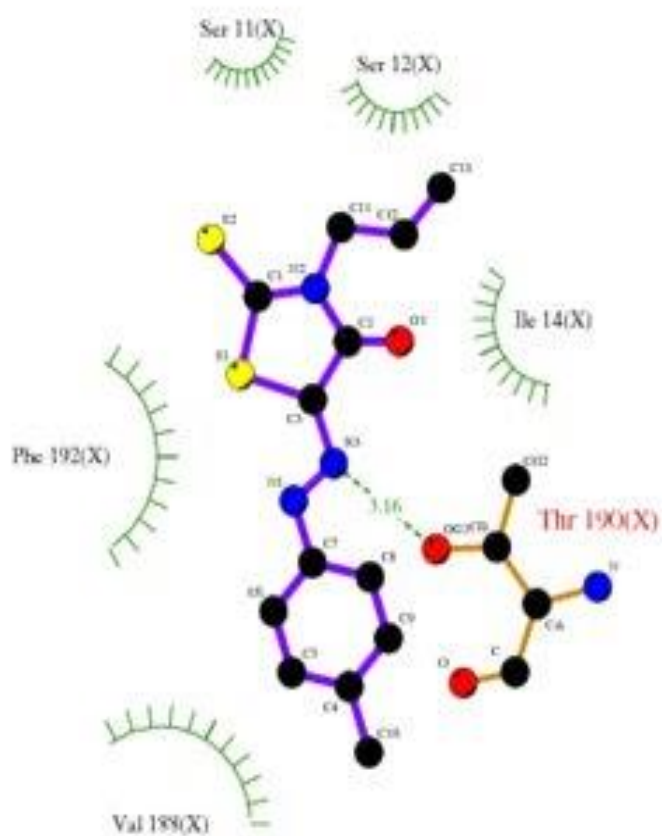
## Key

-  Ligand bond
-  Non-ligand bond
-  Hydrogen bond and its length




-  Non-ligand residues involved in other contact(s)


docking

## Compound (2)



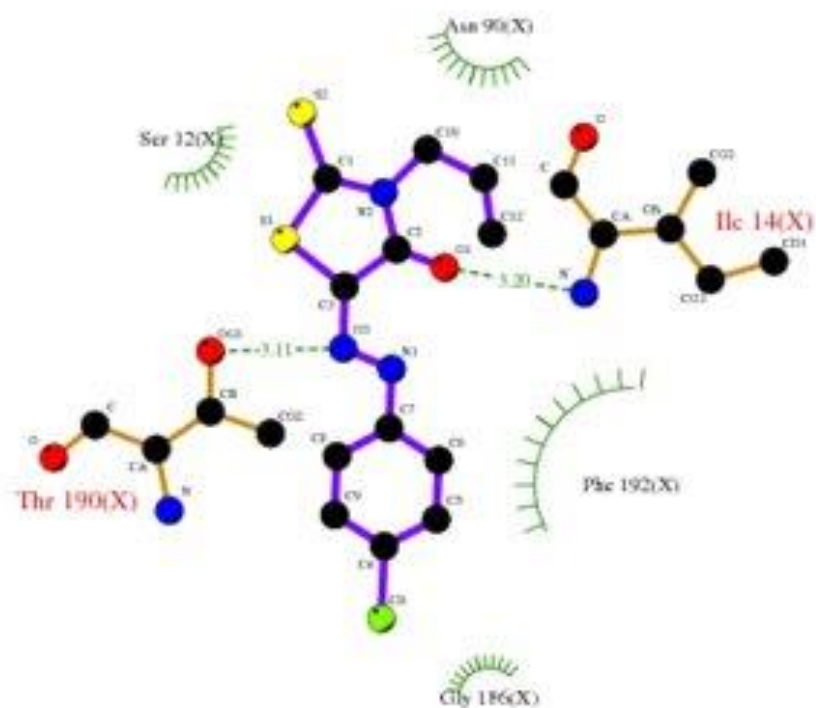
## Key

-  Ligand bond
-  Non-ligand bond
-  Hydrogen bond and its length

 Non-ligand residues involved in other contact(s)

docking

## Compound (3)



## Key

- ● Ligand bond
- ● Non-ligand bond
- ● Hydrogen bond and its length

- His 53 Non-ligand residues involved in other contact(s)

## docking

**Fig. 14.** 2D plot of interaction between allyl rhodanine azode derivatives (1-3) with receptor of breast cancer mutant 3hb5.

## Conclusion

- In 2 M HCl, the allyl rhodanine azodye derivatives stop C- steel from corroding. The Temkin isotherm is fit by the adsorption of allyl rhodanine azodye derivatives.
- The results of DC polarization, AC impedance, and the results of the mass reduction are essentially in good accord with one another and lead to IE with higher inhibitor dose.
- Depending on the polarization value, the utilized inhibitors behave as mixed-kind inhibitors in 2 M HCl.
- When the inhibitor is added, the findings of EIS show a high charge transmission resistance and a low in dual layer capacities, leading to a high IE percent. This is said to rise the dual thickness layer.
- SEM and other procedures were used to compare the morphology of inhibited and uninhibited C-steel (EDX).
- The examined compounds are arranged in the following order: (1) > (2) > (3)
- The data from  $E_{HOMO}$  and  $E_{LUMO}$  that were gathered in the correct order run concurrently to improve in % IE achieved, supporting the earlier sequence.
- The effective centre heteroatom's N and O are of the derivatives of allyl rhodanine azodye, quantum calculation chemistry is produced. By giving electrons to Fe atoms and taking electrons from their third orbital, it can securely adsorb on the surface of Fe.
- The compounds are effective 3hb5-oxidoreductase receptor inhibitors, according to molecular docking and binding energy assays of allyl rhodanine azodye derivatives with breast cancer mutant 3hb5-oxidoreductase receptor.

## References

- [1] M.M. Megahed, M.M. Abdelbar, E.M. Abouelez, A. M. El-Shamy, Egypt. J. Chem., **64** (2021) 5693-5702.
- [2] K.M. Zohdy, A.M. El-Shamy, Atef Kalmouch, Elshafie A.M. Gad, Egypt J. Petrol., **28** (2019) 355-359.
- [3] A. M. El-Shamy, M. Abdelbar, Egypt. J. Chem., **64** (2021) 1867-1876 .
- [4] X. Liu, P.C. Okafor, Y.G. Zheng, Corros. Sci., **51** (2009) 744-751.
- [5] W.M. Saad, A. M. El-Shamy, Bio- and Tribo-Corros., **10** (2024) 14.
- [6] E. A. Ghazy, N. A. Abdel Ghany, Ashraf M. El-Shamy, J. Bio- and Tribo-Corros., **9** (2023) 64.
- [7] Sh.M. Morgan, A.Z. El-Sonbati, H.R. Eissa, Mol. Liq., **240** (2017) 752-776.
- [8] M. M. Megahed, M.Youssef Sedeka, A. M. El-Shamy, Egypt. J. Chem., **63** (2020) 5269-5287.
- [9] A. M. El-Shamy, Egypt. J. Chem., **63** (2020) 5251-5267.
- [10] A.Z. El-Sonbati, M.A. El-Mogazy, S.G. Nozha, M.A. Diab, M.I. Abou-Dobara, A.M. Eldesoky, Sh.M. Morgan, J. Mol. Struct., **1248** (2022) 131498.
- [11] A.Z. El-Sonbati, M.A. Diab, A.M. Eldesoky, Sh.M. Morgan, O.L. Salem, Appl. Organometal. Chem., **33** (2019) e4839.
- [12] M.I. Abou-Dobara, N.F. Omar, M.A. Diab, A.Z. El-Sonbati, Sh.M. Morgan, O.L. Salem, A.M. Eldesoky, Materials Science & Engineering C, **103** (2019) 109727.
- [13] A.Z. El-Sonbati, A.A.M. Belal, M.S. El-Gharib, Sh.M. Morgan, Spectrochim. Acta A, **95** (2012) 627–636.
- [14] A.Z. El-Sonbati, A.A.M. Belal, Sh.M. Morgan, Spectrochim. Acta A, **99** (2012) 353–360.
- [15] M.I. Abou-Dobara, A.Z. El-Sonbati, Sh.M. Morgan, World J. Microbiol. Biotechnol., **29** (2013) 119–126.
- [16] A.Z. El-Sonbati, M.A. Diab, Sh.M. Morgan, Mol. Liq., **225** (2017) 195–206.
- [17] Sh.M. Morgan, A.Z. El-Sonbati, M.A. El-Mogazy, Appl. Organometal. Chem., **32** (2018) e4264
- [18] Sh.M. Morgan, M.A. Diab, A.Z. El-Sonbati, Appl. Organometal. Chem., **32** (2018) e4305.
- [19] Sh.M. Morgan, M.A. Diab, A.Z. El-Sonbati, Appl. Organometal. Chem., **32** (2018) e4281.
- [20] Sh.M. Morgan, N.A. El-Ghamaz, M.A. Diab, J. Mol. Struct., **1160** (2018) 227-241.
- [21] N.A. El-Ghamaz, M.A. Diab, A.Z. El-Sonbati, Sh.M. Morgan, O.L. Salem, Chem. Pap., **71** (2017) 2417-2433.
- [22] J. Zhang, J.X. Liu, W.Z. Yu, Y.G. Yan, L. You, L.F. Liu, Corros. Sci., **52** (2010) 2059-2065.
- [23] G.G. Mohamed, A.A. El-Sherif, M.A. Saad, S.E.A. El-Sawy, Sh.M. Morgan, J. Mol. Liq., **223** (2016) 1311-1332.
- [24] H.M. Refaat, H.A. El-Badway, Sh.M. Morgan, J. Mol. Liq., **220** (2016) 802-812.
- [25] M.A. Diab, A.Z. El-Sonbati, Sh.M. Morgan, M.A. El-Mogazy, Appl. Organometal. Chem., **32** (2018) e4378.
- [26] M.A. Diab, S.G. Nozha, A.Z. El-Sonbati, M.A. El-Mogazy, Sh.M. Morgan, Appl. Organometal. Chem. **33** (2019) e5153.
- [27] M.I. Abou-Dobara, N.F. Omar, M.A. Diab, A.Z. El-Sonbati, Sh.M. Morgan, M.A. El-Mogazy, J. Cell Biochem. **120** (2019) 1667
- [28] A.Z. El-Sonbati, M.A. Diab, Sh.M. Morgan, M.A. El-Mogazy, Appl. Organometal. Chem., **32** (2018) e4530.
- [29] A.Z. El-Sonbati, M.A. Diab, Sh.M. Morgan, A.M. Eldesoky, M.Z. Balboula, Appl. Organometal. Chem., **32** (2018) e4207.
- [30] M.A. Diab, A.Z. El-Sonbati, N.A. El-Ghamaz, Sh.M. Morgan, O. El-Shahat, Eur. Polym J., **115** (2019) 268-281.
- [31] N.A. El-Ghamaz, A.Z. El-Sonbati, Sh.M. Morgan, J. Mol. Struct., **1027** (2012) 92-98.
- [32] A.Z. El-Sonbati, M.A. Diab, A.A. El-Bindary, A.M. Eldesoky, Sh.M. Morgan, Spectrochim. Acta A, **135** (2015) 774-791.

- [33] A.N. Wiercinska, G. Dalmata, *Electrochim. Acta*, **51** (2006) 6179-6185.
- [34] A. Yurt, A. Balaban, S.U. Kandemir, G. Bereket, B. Erk, *Mater. Chem. Phys.*, **85** (2004) 420-426.
- [35] A.Y. Etre, *Appl. Surf. Sci.*, **252** (2006) 8521-8525.
- [36] W.J. Lorenz, F. Mansfeld, *Corros. Sci.*, **21** (1981) 647-672.
- [37] I.N. Putilova, S.A. Balezin, V.P. Barannik, "Metallic Corrosion Inhibitors Pergamon" Press New York, 1960.
- [38] K.K. Al-Neami, A.K. Mohamed, I.M. Kenawy, A.S. Fouda, *Monatsh. Chem.*, **126** (1995) 369-376.
- [39] E.A. Noor, *Int. J. Electrochem. Sci.*, **2** (2007) 996-1017.
- [40] J. Marsh, *Advanced Organic Chemistry 3rd Ed.* Wiley Eastern New Delhi (1988).
- [41] S. Martinez, I. Stern, *Appl. Surf. Sci.*, **199** (2002) 83-89.
- [42] M.A. Al-Khaldi, K.Y. Al-qahtani, *J. Mater. Environ. Sci.*, **4** (5) (2013) 593-600.
- [43] J.W. Schlitz, K. Wippermann, *Electrochim. Acta* **32** (1987) 823-831.
- [44] D.C. Silverman, J.E. Carrico, *Corrosion*, **44** (1988) 280-287.
- [45] D.D. Macdonald, M.C.H. Mckubre, "Impedance measurements in electrochemical systems" *Modern Aspects of Electrochemistry*, J.O'M. Bockris, B.E. Conway, R.E. White, Eds., Plenum Press, New York (1982) pp. 61.
- [46] F. Mansfeld, *Corrosion*, **36** (1981) 301-307.
- [47] C. Gabrielli, "Identification of Electrochemical processes by Frequency Response Analysis" Solarton Instrumentation Group, 1980.
- [48] M. El Achouri, S. Kertit, H.M. Gouttaya, B. Nciri, Y. Bensouda, L. Perez, M.R. Infante, K. Elkacemi, *Prog. Org. Coat.*, **43** (2001) 267-273.
- [49] A. Anejjar, A. Zarrouk, R. Salghi, H. Zarrok, D. Ben Hmamou, B. Hammouti, B. Elmahi, S.S. Al-Deyab, *J. Mater. Environ. Sci.*, **4** (2013) 583-592.
- [50] S.F. Mertens, C. Xhoffer, B.C. Decooman, E. Temmerman, *Corrosion*, **53** (1997) 381-388.
- [51] G. Trabanelli, C. Montecelli, V. Grassi, A. Frignani, *J. Cem. Concr. Res.*, **35** (2005) 1804-1813.
- [52] A.J. Trowsdate, B. Noble, S.J. Haris, I.S.R. Gibbins, G.E. Thomson, G.C. Wood, *Corros. Sci.*, **38** (1996) 177-191.
- [53] F.m. Reis, H.G. de Melo, I. Costa, *J. Electrochem. Acta*, **51** (2006) 1780-1788.
- [54] M. Lagrenée, B. Mernari, M. Bouanis, M. Traisnel, F. Bentiss, *Corros. Sci.*, **44** (2002) 573-588.
- [55] E. McCafferty, N. Hackerman, *J. Electrochem. Soc.*, **119** (1972) 999-1009.
- [56] H. Ma, S. Chen, L. Niu, S. Zhao, S. Li, D. Li, *J. Appl. Electrochem.*, **32** (2002) 65-72.
- [57] E. Kuş, F. Mansfeld, *Corros. Sci.*, **48** (2006) 965-979.
- [58] G.A. Caignan, S.K. Metcalf, E.M. Holt, *J. Chem. Cryst.*, **30** (2000) 415-422.
- [59] A. M. El-Shamy, Y. Reda, K. M. Zohdy, Ashraf K. Eessaa, *Egypt. J. Chem.*, **63** (2020) 579-597.
- [60] Sh.M. Morgan, M.A. Diab, A.Z. El-Sonbati, *Appl. Organomet. Chem.*, **32** (2018) e4504.
- [61] A.Z. El-Sonbati, M.A. Diab, Sh.M. Morgan, M.Z. Balboula, *Applied Organometal. Chem.*, **32** (2018) e4059.
- [62] A.Z. El-Sonbati, M.A. Diab, Sh.M. Morgan, S.Y. Abbas, G.G. Mohamed, *Inorganic Chem. Comm.*, **137** (2022) 109193.
- [63] M.A. Diab, G.G. Mohamed, W.H. Mahmoud, A.Z. El-Sonbati, Sh.M. Morgan, S.Y. Abbas, *Appl. Organometal. Chem.*, **33** (2019) e4945.
- [64] A.Z. El-Sonbati, W.H. Mahmoud, G.G. Mohamed, M.A. Diab, Sh.M. Morgan, S.Y. Abbas, *Appl. Organometal. Chem.*, **33** (2019) e5048.
- [65] A. Z. El-Sonbati, M. A. Diab, Sh.M. Morgan, H.A Seyam, *J. Mol. Struct.*, **1154** (2018) 354-365.
- [66] A.Z. El-Sonbati, M.A. Diab, Sh.M. Morgan, M.I. Abou-Dobara, A.A. El-Ghettany, *Mol. Struct.* **1200** (2020) 127065
- [67] M.A. Diab, A.Z. El-Sonbati, E.A. Gomma, M.A. El-Mogazy, Sh.M. Morgan, M.I. Abou-Dobara, N.F. Omar, M.M. El-Zahed, M.A. Osman. *J. Iranian Chem. Soc.*, **19** (2022) 3079-3102.
- [68] A.Z. El-Sonbati N.F. Omar, M.I. Abou-Dobara, M.A. Diaba, M.A. El-Mogazy, Sh.M. Morgan, M.A. Hussien, A.A. El-Ghettany, *J. Mol. Struct.*, **1239** (2021) 130481.
- [69] A.Z. El-Sonbati, M.A. Diab, S. Y. Abbas, Gehad G. Mohamed, Sh.M. Morgan, *Egypt J. Chem.*, **64** (2021) 4125 - 4136.
- [70] A.Z. El-Sonbati, M.A. Diab, Sh.M. Morgan, S. Y. Abbas, Gehad G. Mohamed, Ehab M. Zayed, *Egyptian Journal of Chemistry*, **66** (2023) 1879-1891.
- [71] M.M. El-Zahed, M.A. Diab, A.Z. El-Sonbati, S.G. Nozha, H.R. Issa, M.A. El-Mogazy, Sh.M. Morgan, *Mat. Sci. Eng. B*, **299** (2024) 116998.